Characterization of Ba2In2-xSnxO5+x/2 oxide ion conductors

Aurélie Rolle, Helen Seymour, Pascal Roussel, Annick Rubbens, Rose-Noëlle Vannier

Characterization of $Ba_2In_{2-x}Sn_xO_{5+x/2}$ oxide ion conductors

Aurélie Rolle*, Helen Seymour, Pascal Roussel, Annick Rubbens, Rose-Noëlle Vannier

UCCS - Unité de Catalyse et Chimie du Solide, Equipe de Chimie du Solide,

ENSCL / UST Lille 1, BP 90 108, 59652 Villeneuve d'Ascq Cedex, France

Abstract

The $Ba_2In_{2-x}Sn_xO_{5+x/2}$ solid solution was confirmed up to x = 1 by solid state reaction. X-ray diffraction at room and at elevated temperatures, Raman scattering and impedance spectroscopy were used to characterise the samples. Structure refinement of composition x = 0.1 from neutron diffraction data reveals that tin is preferentially located in the tetrahedral layers of the brownmillerite.

Keywords: oxide ion conductors, $Ba_2In_{2-x}Sn_xO_{5+x/2}$, X-ray diffraction, neutron diffraction, Raman scattering.

* Corresponding author

Aurélie Rolle

UCCS - Unité de Catalyse et Chimie du Solide, Equipe de Chimie du Solide,

CNRS UMR 8181, ENSCL / UST Lille 1, BP 90108, 59652 Villeneuve d'Ascq Cedex, France

Tel: +33 (0) 3 20 43 49 73, Fax: +33 (0) 3 20 43 68 14

E-mail: Aurelie.Rolle@ensc-lille.fr

1. Introduction

Goodenough *et al.* reported in 1990 fast oxide ion conduction in $Ba_2In_2O_5$ above 925°C [1], making it of potential use in applications such as solid oxide fuel cells, oxygen generating systems and dense catalytic membrane reactors. At room temperature, its structure is of brownmillerite-type. Its symmetry is orthorhombic and it can be described as a defective perovskite composed of alternating octahedral and tetrahedral layers [2-4]. When the temperature is increased, the symmetry becomes tetragonal (T>925°C) and then cubic (T>1040°C). These high temperature forms are purely oxide ion conductive.

Several attempts have been made to stabilise the tetragonal and cubic forms at lower temperatures by partial substitution for barium or indium. On the barium site, Sr [8, 11, 21, 22], La [11, 22-28], Pb [29] have been partially incorporated. A wide range of elements have been incorporated on the indium site: Cu [2, 5, 6], Ga [3, 7-11], Y [7, 11, 12], Yb [17], Sc [7, 12], Al [9], Ce [2, 12, 13], Zr [1, 14-16], Si [12], Ti [17], Sn [18], W [19, 20], Mo [20], V [20], Ta [12, 20] and Nb [12, 20]. However, the precise site-occupancy (tetrahedral versus octahedral indium sites) was not always examined.

The aim of the present paper is the characterisation of the $Ba_2In_{2-x}Sn_xO_{5+x/2}$ solid solution. A range of compositions was examined to determine its solubility limit and neutron diffraction was performed to determine the preferred site for this dopant.

2. Experimental

$Ba_2In_{2-x}Sn_xO_{5+x/2}$ compounds were prepared by solid state reaction at 1300°C from stoichiometric amounts of binary oxides and carbonates with intermediate grindings after annealing at 1000°C and 1200°C, in alumina crucibles. Since these phases are known to be sensitive to humidity, powders were dried at 500°C under a flow of dry air before characterisation. Next, they were characterized by X-ray diffraction using a Hüber diffractometer equipped with an image plate sensitive detector over the range 10-100° in 2θ with a time of 15 min ($Cu_{K\alpha 1}$ = 1.54056 Å). Raman spectra were recorded at room temperature using the 647.1 nm excitation line from a Spectra Physics krypton ion laser. The beam was focused onto the sample using the macroscopic configuration of the apparatus. The scattered light was analysed with an XY Raman Dilor spectrometer equipped with an optical multichannel charge coupled device liquid nitrogen–cooled detector. Acquisition and data processing were performed with the software LABSPEC.

The structure was refined from neutron diffraction data, collected at room temperature on the high resolution powder diffractometer D2B at the Institut Laue Langevin (I.L.L.) at Grenoble (λ = 1.59334 Å). To collect data in air, approximately 20g of powder were introduced in a quartz tube, which was open at one end. The data were collected over the range 0.3-160° with a 0.05° step. The JANA 2000 software [30], option powder, was used for the refinement. The Rietveld method was applied. The profile could be fitted to a pseudo-Voigt function and the background was determined manually.

High temperature X-ray diffraction was performed on a Bruker axs D8 Advance diffractometer equipped with a high temperature Anton Paar HTK 1200 N chamber and a one dimensional X-ray detector (VÅNTEC-1) using $Cu_{K\alpha}$ radiation. Data were collected in over the range10-80° in 2θ, with a 0.015° step and a time of 0.2 seconds per step from room temperature to 1000°C. Diffractograms were obtained every 25°C on heating and cooling with a heating and cooling rate of 0.1°C/sec. Samples were deposited on platinum sheets to avoid any contamination with the alumina crucible.

Conductivity measurements were performed on pellets 5 mm in diameter and 2-3 mm in thickness. Platinum paste electrodes were painted on both faces. Samples were annealed at 850°C prior to measurement. Measurements were taken using a SI 1255 response analyser (Solartron) in the 1-10^6 Hz frequency range from 500°C to 875°C for compositions x = 0.1 and x = 0.2 and 500°C to 1000°C for compositions x = 0 and x = 0.3 every 20°C with 1h equilibration times before each measurement.

3. Results and discussion

3.1. $Ba_2In_{2-x}Sn_xO_{5+x/2}$ solid solution

X-ray diffractograms obtained for several compositions are presented in Fig. 1. It reveals a solid solution for substitution ratio up to x = 1, beyond which $BaSnO_3$, appeared as an impurity. For $x \leq 0.2$, the structure is orthorhombic. The composition x = 0.3 contains a mixture of orthorhombic and tetragonal phases, whereas composition x = 0.4 is a mixture of tetragonal and cubic phases. For $0.4 \leq x < 1$, at room temperature, the sample consists of a single cubic phase in good agreement with data previously reported for composition x=1, studied for its protonic properties [18].

Raman scattering was performed on compositions x = 0, 0.1, 0.2, 0.3, 0.35, 0.4, 0.5 and 0.6. The spectra are given in Fig. 2 and confirm the change in symmetry with increasing dopant content. Compositions with $x \leq 0.2$, contain a single brownmillerite-type orthorhombic phase and show similar spectra. The unresolved bands obtained for composition x = 0.3 are in agreement with the mixture of orthorhombic and tetragonal structures. Important spectral modifications are observed for composition in the range of $0.3 \leq x \leq 0.4$. The bands broaden as the substitution ratio is increased with a shift in the frequency (607 cm^{-1} and 635 cm^{-1} for x = 0.3 and 0.4 respectively). This broadening, which is more intense for cubic composition, indicates an increasing disorder as the substitution ratio is increased and the frequency shift characterises the solid solution evolution. An increase in the intensity of bands at 393 cm^{-1} and $\approx$ 700 cm^{-1} is also noticeable as the substitution rate increases; this is likely a result of the dopant changing the local structure. Work is currently in progress to determine the exact nature of the changes.

3.2. Dopant location in the brownmillerite structure

To determine the preferred location of the Sn dopant in the brownmillerite unit cell, neutron diffraction data were collected for composition x = 0.1. The Icmm structural model proposed by Berastegui was used for the refinement [16]. In a previous study, we determined that the excess oxygen in a molybdenum doped compound was located at 4c (¼, ¼, ¼) [31]. We therefore introduced this extra site to the refinement to account for the oxygen over-stoichiometry. The sum of the oxygen occupancies was constrained to match the expected oxygen stoichiometry and the occupancy independently refined. O(3) is a split position and its occupancy cannot be higher than 0.5. Since it converged slightly to a higher value, it was constrained to 0.5. As a first step, tin was introduced to both indium sites of the brownmillerite structure, In(1) corresponding to the octahedral layers and In(2) to the tetrahedral layers, while constraining the sum of their occupancies to be equal to the expected stoichiometry. The refinement revealed a clear preference for the In(2) site with an occupancy of –0.031(5) for the In(1) site. For the final refinement all the Sn dopant was therefore placed on the In(2) site. The results of the refinement are given in Table 1. A comparison of the calculated profile and experimental data is given in Fig. 3. A good fit was obtained with the following reliability factors: R_{obs} = 2.80%, R_{wobs} = 2.70%, R_p = 3.26%, R_{wp} = 4.10%, R_F = 2.80% and R_{wF} = 2.70%. Sn is therefore distributed over the tetrahedral layers of the brownmillerite-type structure. The same trend was observed for Ti-doped compounds [17]. In

addition, the refinement confirmed that the extra oxygen is situated on 4c, with an occupancy of 0.16(2) and a high isotropic thermal displacement of 0.11(2). This later value was a result of a small occupancy and therefore greater relative error for this position. Oxygen vacancies on O(1) (equatorial oxygen site in the octahedral layers) and O(2) sites (apical oxygen site) were also evidenced. These oxygen vacancies indicate that a disordering of the oxygen lattice begins at a lower temperature than the undoped compound and suggests that the phase transition temperature of the Sn-doped compound, associated with an increase of the conductivity, should occur at lower temperature.

3.3. Phase transition

To characterise the phase transitions in this compound (x = 0.1), X-ray diffraction was performed at different temperatures. The results are given in Fig. 4. The disappearance of the small peak at 33.5°, characteristic of the orthorhombic superstructure, as well as the shrinkage of the main Bragg peaks indicate a transition to the tetragonal form at 750°C. At 1000°C, all the superlattice reflections vanish, indicating the structure has transformed fully to the cubic phase. The phase transitions are fully reversible on cooling, thereby confirming the stabilisation of the cubic and tetragonal forms to lower temperature compared to undoped $Ba_2In_2O_5$. The decrease of the orthorhombic-tetragonal phase transition with the substitution ratio is in good agreement with our previous results on vanadium, molybdenum and tungsten doped compounds [20], it also confirms the trend observed by Fisher *at al.* when In^{3+} was substituted with elements of same valence but having smaller ionic radius [6].

3.4. Conduction properties

Arrhenius plots of the conductivity, measured under dry air for compositions x = 0.1, x = 0.2 and x = 0.3, are compared to that of the undoped compound in Fig. 5. Relative densities of the samples are given in brackets. These materials are difficult to densify, so that pellets with relative densities of only 77% for x = 0.1 and x = 0.2 compositions and 75% for the parent compound were used. For composition x = 0.3, the relative density was only 64%. With such relative densities, the conduction properties trend only can be deduced. Similar activation energies of about 1eV were observed at high temperature for all compositions, typical of the high temperature forms of $Ba_2In_2O_5$. High conductivities were observed for the tetragonal form up to 750°C for composition x = 0.1. The orthorhombic-tetragonal phase

transition is more sluggish for composition x = 0.2 and characterised by a higher activation energy below 650°C. Lower conductivities were obtained for composition x = 0.3 in part due to the lower relative density of the pellet.

4. Conclusions

The $Ba_2In_{2-x}Sn_xO_{5+x/2}$ solid solution extends up to x = 1. The structure remains orthorhombic at room temperature up to x = 0.2 with tin distributed over the tetrahedral layers as evidenced by neutron diffraction. The partial replacement of indium with tin results in a decrease of the temperature of the order-disorder phase transition temperature from orthorhombic to tetragonal symmetry, and cubic forms are stabilised at room temperature for composition with x > 0.4.

Acknowledgements

The Institut Laue Langevin is thanked for providing neutron facilities and Dr. Emmanuelle Suard (Institut Laue Langevin) and Dr. Olivier Mentré are gratefully acknowledged for their help in the data collection. The authors are very grateful to L. Burylo for help with the X-ray diffraction. The Fonds Européen de Développement Régional (FEDER), Centre National de la Recherche Scientifique (CNRS), Région Nord Pas-de-Calais and the Ministère de l'Education Nationale, de l'Enseignement Supérieur et de la Recherche » are acknowledged for funding of X-ray diffractometers. A. R. is also grateful to the CNRS and the Région Nord Pas-de-Calais for the funding of her PhD grant. Finally, the authors are very grateful to Prof. M.S. Islam and Dr. C.A.J. Fisher for fruitful discussion and English corrections.

References

[1] Goodenough J. B. , Ruiz-Diaz J. E., Zhen Y. S. (1990) Solid State Ionics 44:21-31.

[2] Gregory D. H., Weller M. T. (1993) J. Solid State Chem. 107(1):134-148.

[3] Adler S. B., Reimer J. A., Baltisberger J., Werner U. (1994) J. Am. Chem. Soc. 116:675-681.

[4] Speakman S. A., Richardson J. W., Mitchell B. J., Misture S. T. (2002) Solid State Ionics 149:247-259.

[5] Kambe S., Shime I., Ohshima S., Okuyama K., Ohnishi N., Hiraga K. (1994) Physica C 220:119-126.

[6] Kharlanov A. L., Khasanova N. R., Paromova M. V., Antipov E. V., Lykova L. N., Kovba L. M. (1990) Russ. J. Inorg. Chem. 35 (12):1741-1743.

[7] Fisher C. A. J., Derby B., Brook R. J. (1996) Br. Ceram. Proc. 56:25-33.

[8] Yamamura H., Yamada Y., Mori T., Atake T. (1998) Solid State Ionics 108:377-381.

[9] Yamamura H., Hamazaki H., Kakinuma K., Mori T., Haneda H. (1999) J. Korean Phys. Soc. 35:200-204.

[10] Yao T., Uchimoto Y., Kinuhata M., Inagaki T., Yoshida H. (2000) Solid State Ionics 132:189-198.

[11] Kakinuma K., Yamamura H., Atake T. (2002) J. Therm. Anal. Calorim. 69:897-904.

[12] Yamaji A., Kawakami K., Arai M., Adachi T. (2000) Mat. Res. Soc. Symp. 575 :343-348.

[13] Kendall K. R., Navas C., Thomas J. K., zur Loye H. C. (1995) Solid State Ionics 82:215-223.

[14] Manthiram A., Kuo J. F., Goodenough J. B. (1993) Solid State Ionics 62:225-234.

[15] Goodenough J. B., Manthiram A., Kuo J. F. (1993) Mater. Chem. Phys. 35:221-224.

[16] Berastegui P., Hull S., Garcia-Garcia J., Eriksson S. G. (2002) J. Solid State Chem. 164:119-130.

[17] Jayaraman V., Magrez A., Caldes M., Joubert O., Ganne M., Piffard Y., Brohan L. (2004) Solid State Ionics 170(1-2):17-24.

[18] Schober T. (1998) Solid State Ionics 109:1-11.

[19] Shimura T., Yogo T. (2004) Solid State Ionics 175:345-348.

[20] Rolle A., Giridharan N. V., Vannier R. N., Abraham F. (2005) Solid State Ionics 176:2095-2103.

[21] Yoshinaga M., Yamaguchi M., Furuya T., Wang S., Hashimoto T. (2004) Solid State Ionics 169:9-13.

[22] Kakinuma K., Yamamura H., Haneda H., Atake T. (2002) Solid State Ionics 154-155:571-576.

[23] Kakinuma K., Yamamura H., Haneda H., Atake T. (1999) J. Therm. Anal. Calorim. 57:737-743.

[24] Uchimoto Y., Yao T., Takagi H., Inagaki T., Yoshida H. (2000) Electrochemistry 68:531-533.

[25] Kakinuma K.,Yamamura H., Haneda H., Atake T. (2001) Solid State Ionics 140:301-306.

[26] Liu Y., Withers R. L., Gerald J. F. (2003) J. Solid State Chem. 170:247-254.

[27] Kakinuma K., Takahashi N., Yamamura H., Nomura K., Atake T. (2004) Solid State Ionics 168:69-74.

[28] Goodenough J. B. (1997) Solid State Ionics 94:17-25.

[29] Kuramochi H., Mori T., Yamamura H., Kobayashi H., Mitamura T. (1994) J. Ceramic Soc. Japan 102:1160-1163.

[30] Petricek V., Dusek M., Palatinus L., *The crystallographic computing system JANA 2000*, Institute of Physics: Praha, Czech Republic, 2006.

[31] Rolle A., Roussel P., Giridharan N. V., Suard E., Vannier R. N., Chem. Mater., submitted.

Paper presented at the 11th EuroConference on the Science and Technology of Ionics, Batz-sur-Mer, Sept. 9 - 15, 2007

Table captions

Table 1. Structural model for composition x = 0.1, described in the Icmm space group, from neutron diffraction data collected at room temperature.

Figure Captions

Fig. 1. $Ba_2In_{2-x}Sn_xO_{5+x/2}$ X-ray diffractograms for compositions $0 \leq x \leq 1.2$ (* indicate the impurity $BaSnO_3$).

Fig. 2. Raman spectra of $Ba_2In_{2-x}Sn_xO_{5+x/2}$ phases with x = 0, 0.1, 0.2, 0.3, 0.35, 0.4, 0.5, 0.6.

Fig. 3. Calculated profile of $Ba_2In_{1.9}Sn_{0.1}O_{5.05}$ compared to experimental neutron diffraction data collected at room temperature.

Fig. 4. High temperature X-ray diffraction data for $Ba_2In_{1.9}Sn_{0.1}O_{5.05}$ upon a) heating and b) cooling.

Fig. 5. Arrhenius plots for $Ba_2In_{2-x}Sn_xO_{5+x/2}$ with x = 0, 0.1, 0.2, 0.3. Relative density of pellets are given in brackets.

Table 1. Structural model for composition x = 0.1, described in the Icmm space group, from neutron diffraction data collected at room temperature.

Icmm	**A (Å)**	**b (Å)**	**c (Å)**	**volume (Å^3)**	**density**
	6.0552(4)	16.7696(8)	5.9566(4)	604.85(7)	6.43(2)

Atom	**Site**	**x**	**y**	**z**	**Occupancy**	**U_{iso} (Å^2)**
Ba	8h	0.5076(5)	0.6099(2)	0	1	0.0284(6)
In(1)	4a	0	0	0	1	0.0206(9)
In/Sn(2)	8i	0.5584(8)	¼	0.523(2)	0.45	0.035(2)
O(1)	8g	¼	0.9925(2)	¼	0.978(9)	0.0258(6)
O(2)	8h	0.0451(4)	0.1361(2)	0	0.965(9)	0.0363(7)
O(3)	8i	0.6327(8)	¼	0.138(1)	0.5	0.041(2)
O(4)	4c	¼	¼	¼	0.16(2)	0.11(2)

Fig 1. $Ba_2In_{2-x}Sn_xO_{5+x/2}$ X-ray diffractograms for compositions $0 \leq x \leq 1.2$ (* indicates the impurity $BaSnO_3$).

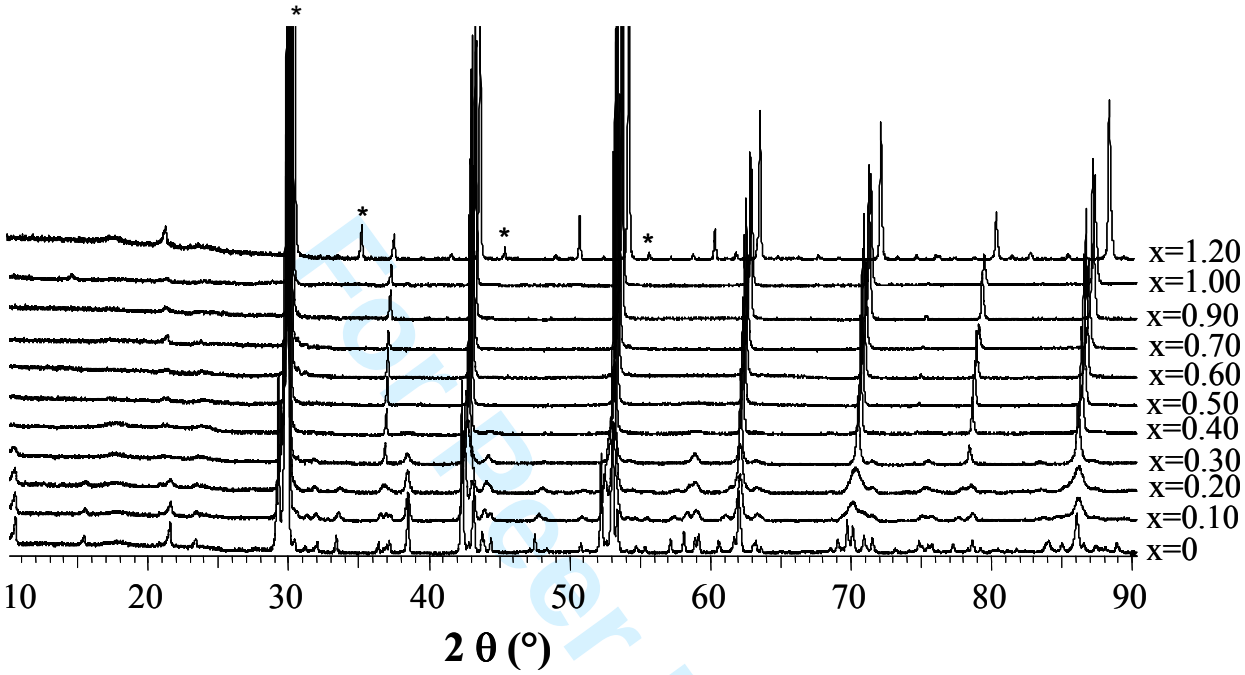

Fig. 2. Raman spectra of $Ba_2In_{2-x}Sn_xO_{5+x/2}$ phases with x = 0, 0.1, 0.2, 0.3, 0.35, 0.4, 0.5, 0.6.

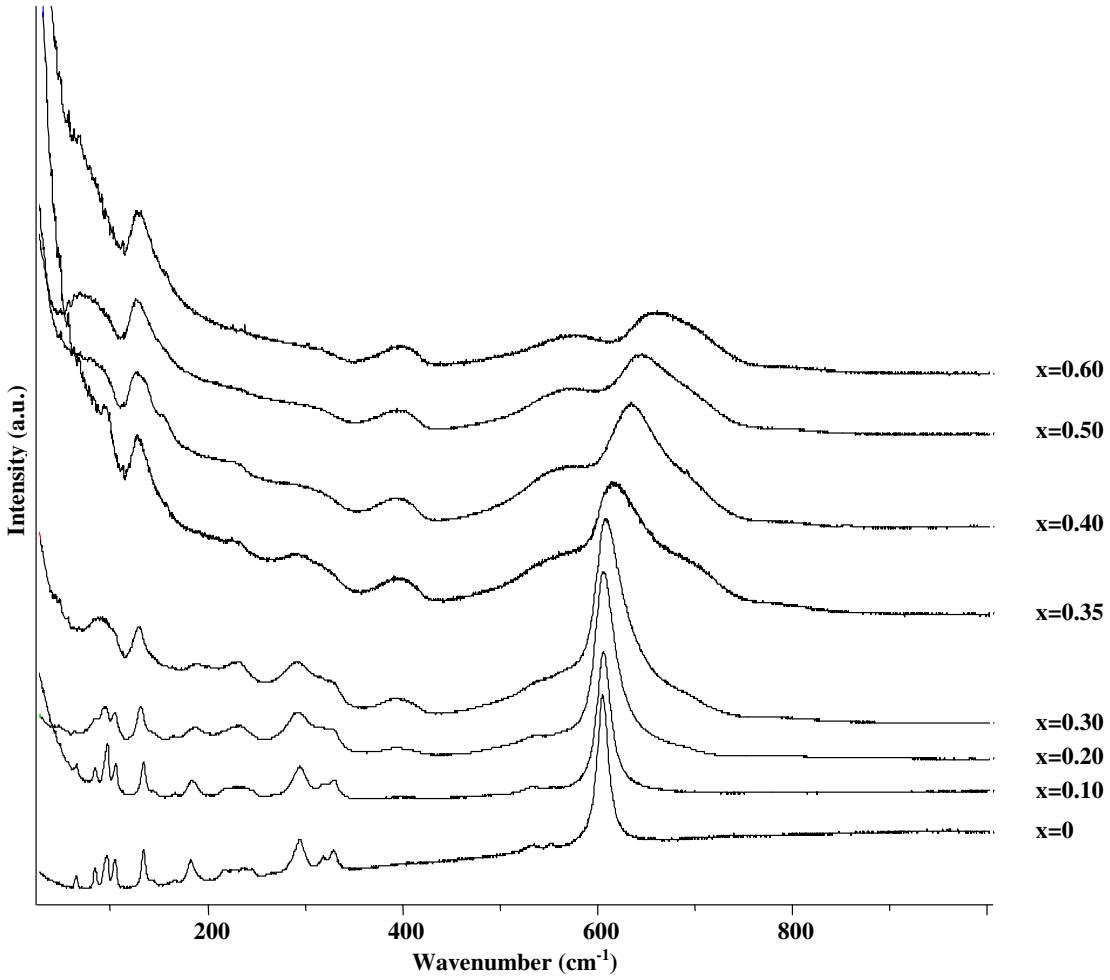

Fig. 3. Calculated profile of $Ba_2In_{1.9}Sn_{0.1}O_{5.05}$ compared to experimental neutron diffraction data collected at room temperature.

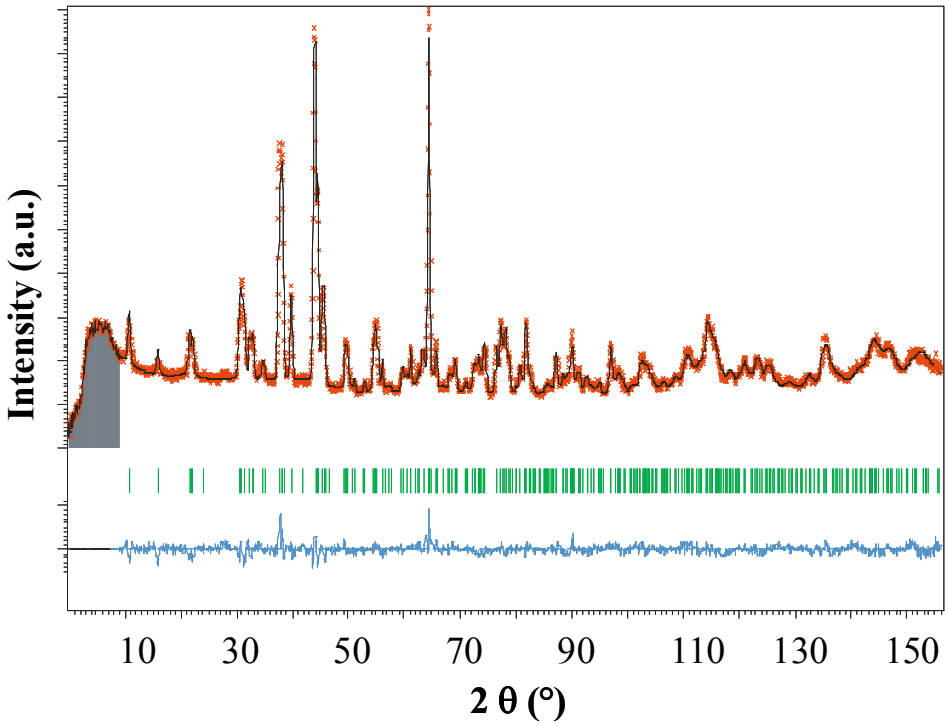

Fig. 4. High temperature X-ray diffraction data for $Ba_2In_{1.9}Sn_{0.1}O_{5.05}$ upon a) heating and b) cooling.

a)

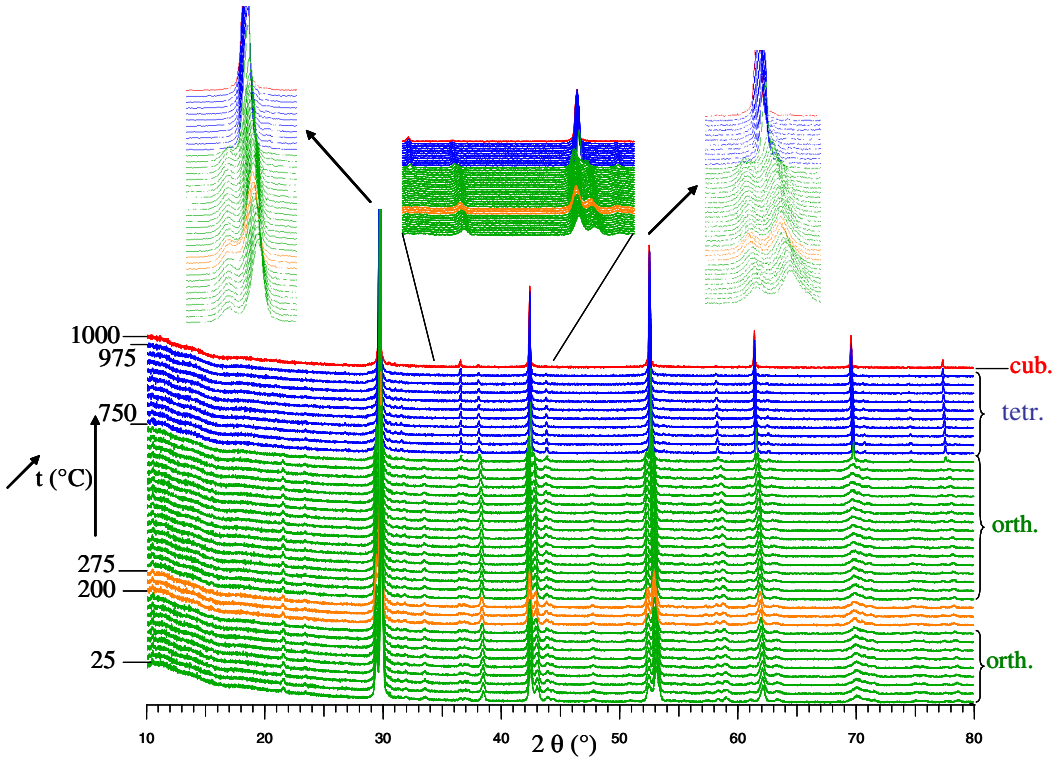

b)

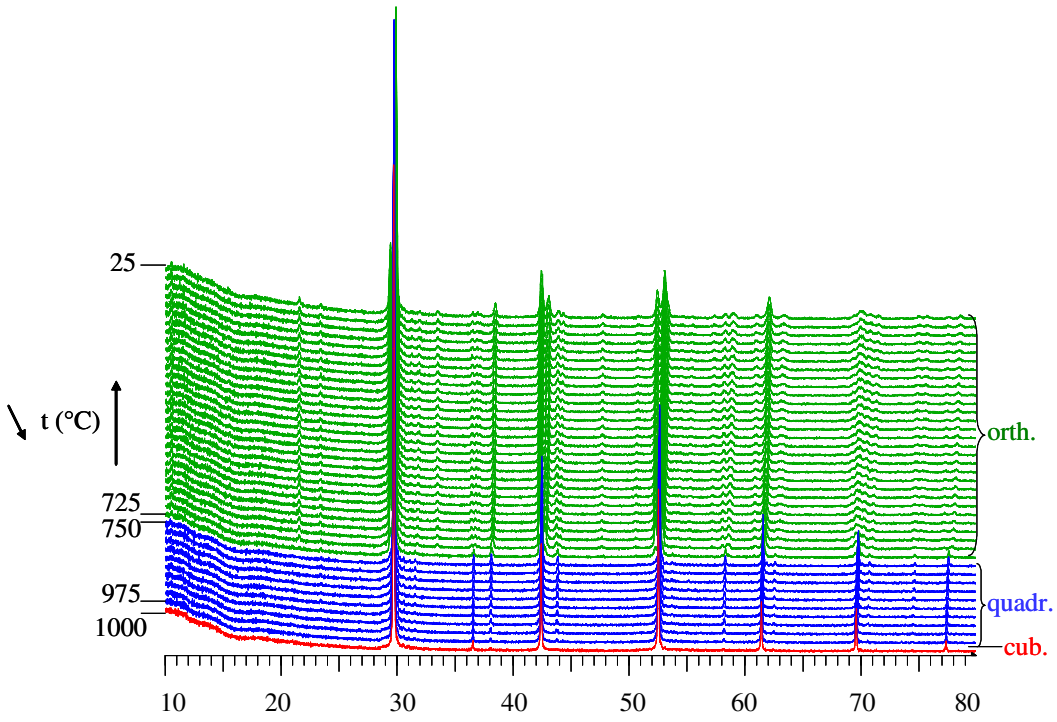

Fig. 5. Arrhenius plots for $Ba_2In_{2-x}Sn_xO_{5+x/2}$ with x = 0, 0.1, 0.2, 0.3. Relative densities of pellets are given in brackets.